Transient brightening of Jupiter's aurora observed by the Hisaki satellite and Hubble Space Telescope during approach phase of the Juno spacecraft

T. Kimura[1] ID, J. D. Nichols[2] ID, R. L. Gray[3] ID, C. Tao[4] ID, G. Murakami[5] ID, A. Yamazaki[5] ID, S. V. Badman[3] ID, F. Tsuchiya[6] ID, K. Yoshioka[7] ID, H. Kita[6] ID, D. Grodent[8] ID, G. Clark[9] ID, I. Yoshikawa[10] ID, and M. Fujimoto[5,11]

[1]Nishina Center for Accelerator-Based Science, RIKEN, Saitama, Japan, [2]Department of Physics and Astronomy, University of Leicester, Leicester, UK, [3]Department of Physics, Lancaster University, Lancaster, UK, [4]National Institute of Information and Communications Technology, Tokyo, Japan, [5]Institute of Space and Astronautical Science, Japan Aerospace Exploration Agency, Sagamihara, Japan, [6]Planetary Plasma and Atmospheric Research Center, Tohoku University, Sendai, Japan, [7]Department of Earth and Planetary Science, Graduate School of Science, University of Tokyo, Tokyo, Japan, [8]Laboratory for Planetary and Atmospheric Physics, Université de Liège, Liège, Belgium, [9]The Johns Hopkins University Applied Physics Laboratory, Laurel, Maryland, USA, [10]Department of Complexity Science and Engineering, University of Tokyo, Kashiwa, Japan, [11]Earth-Life Science Institute, Tokyo Institute of Technology, Tokyo, Japan

Abstract In early 2014, continuous monitoring with the Hisaki satellite discovered transient auroral emission at Jupiter during a period when the solar wind was relatively quiet for a few days. Simultaneous imaging made by the Hubble Space Telescope (HST) suggested that the transient aurora is associated with a global magnetospheric disturbance that spans from the inner to outer magnetosphere. However, the temporal and spatial evolutions of the magnetospheric disturbance were not resolved because of the lack of continuous monitoring of the transient aurora simultaneously with the imaging. Here we report the coordinated observation of the aurora and plasma torus made by Hisaki and HST during the approach phase of the Juno spacecraft in mid-2016. On day 142, Hisaki detected a transient aurora with a maximum total H_2 emission power of ~8.5 TW. The simultaneous HST imaging was indicative of a large "dawn storm," which is associated with tail reconnection, at the onset of the transient aurora. The outer emission, which is associated with hot plasma injection in the inner magnetosphere, followed the dawn storm within less than two Jupiter rotations. The monitoring of the torus with Hisaki indicated that the hot plasma population increased in the torus during the transient aurora. These results imply that the magnetospheric disturbance is initiated via the tail reconnection and rapidly expands toward the inner magnetosphere, followed by the hot plasma injection reaching the plasma torus. This corresponds to the radially inward transport of the plasma and/or energy from the outer to the inner magnetosphere.

1. Introduction

Structures of Jupiter's aurora are roughly categorized into four components: the main oval emission, poleward emission, outer emission, and satellite-induced emissions [see *Clarke et al.*, 2004; *Grodent*, 2015, and the references therein]. The main oval is thought to be driven via field-aligned particle acceleration associated with a magnetosphere-ionosphere coupling current system corresponding to the middle magnetosphere (10–40 Jovian radii, R_J [*Khurana et al.*, 2004]) [e.g., *Hill*, 1979, 2001; *Cowley and Bunce*, 2003a, 2003b]. The poleward emission within the main oval is associated with the outer magnetosphere (>40 R_J) and also with the external solar wind [e.g., *Pallier and Prangé*, 2001, 2004; *Waite et al.*, 2001; *Grodent et al.*, 2004; *Bonfond et al.*, 2016]. The outer emission that surrounds the main oval with both diffuse and discrete morphologies [e.g., *Mauk et al.*, 2002; *Radioti et al.*, 2009] is associated with the energetic particle dynamics (e.g., injections and pitch angle scattering of the energetic particles) in the inner magnetosphere (<10 R_J) [*Tomás et al.*, 2004; *Dumont et al.*, 2014]. The satellite-induced emissions are excited by current systems that electromagnetically couple the satellites with Jupiter.

Continuous monitoring by the Hisaki satellite recently demonstrated recurrence of the transient aurora with a typical duration of 3–11 h during a period when the solar wind was relatively quiet [*Kimura et al.*, 2015], a phenomenon which has appeared in previous observations by the International Ultraviolet Explorer and

Cassini [*Prangé et al.*, 2001; *Pryor et al.*, 2005; *Tsuchiya et al.*, 2010]. The occurrence of the transient aurora during quiet solar wind periods suggests that "internal" processes, e.g., Io's volcanic activity [e.g., *Bonfond et al.*, 2012], are likely the dominant driver. In this study, we refer to the aurora that brightens and decays within a few Jupiter rotations as the "transient aurora." *Kimura et al.* [2015] concluded that the transient aurora is part of the global magnetospheric disturbance referred to as the "energetic event" [e.g., *Louarn et al.*, 2014], which is characterized by a 2–3 day recurrence of auroral radio bursts, energetic particle injection in the inner magnetosphere, and a magnetic field perturbation. The work by *Louarn et al.* suggested that the energetic event is initiated by Vasyliūnas tail reconnection [e.g., *Vasyliūnas*, 1983; *Kronberg et al.*, 2007, 2008]. In the Vasyliūnas reconnection process, a closed magnetic field line filled with iogenic plasma is stretched down the tail by the centrifugal force of corotation and pinched off, forming a plasmoid. This is referred to as "internally driven" reconnection [*Kronberg et al.*, 2007] in contrast with Dungey-type reconnection that is "externally driven" by the solar wind.

The simultaneous imaging by the Hubble Space Telescope (HST) with Hisaki indicated that the three structures introduced above, the main oval, poleward emissions, and outer emission, were enhanced simultaneously around the transient aurora [*Kimura et al.*, 2015; *Badman et al.*, 2016; *Gray et al.*, 2016]. However, the temporal and spatial evolutions of the transient aurora and energetic events were not resolved by these previous observations because of the lack of continuous monitoring that spans the typical duration of the transient aurora.

From early- to mid-2016, the Juno spacecraft measured the solar wind with in situ plasma instruments during the approach phase to Jupiter. The simultaneous HST observing campaign spanning from May to July 2016 was analyzed by *Nichols et al.* [2017]. Here we report the continuous monitoring of the aurora and plasma torus made by Hisaki during the HST observing campaign. The temporal evolution of the auroral regions during the transient event is discussed based on the comparison of the Hisaki monitoring with the HST imaging.

2. Data Set

Before and after the Jupiter Orbit Insertion of Juno, Hisaki continuously monitored Jupiter's aurora and plasma torus from 21 January to 30 August 2016 (day of year, DOY, 21–243). This study defines the analysis period from DOY136 to 160, which overlaps the HST observations investigated by *Nichols et al.* [2017].

The continuous monitoring was made with the extreme ultraviolet (EUV) spectrometer, EXCEED, on board Hisaki [*Yoshioka et al.*, 2013; *Yamazaki et al.*, 2014]. The EUV photons emitted from the aurora and torus measured with EXCEED are reduced to spectral imaging data. In the observation period of the present study, the dumbbell-shaped slit was used for imaging spectroscopy (see Figure 1 of *Kimura et al.* [2015]). The slit length along the spatial axis is 360 arcsec, while its width along the wavelength axis is 140 arcsec, narrowed to 20 arcsec at ±45 arcsec from the middle point of the spatial axis. The spectral range spans from 550 to 1450 Å with a resolution of 3 Å full width at half maximum (FWHM). The FWHM of the point spread function (PSF) is ~17 arcsec [*Yamazaki et al.*, 2014; *Yoshioka et al.*, 2013]. Hisaki continuously acquired the imaging spectra during 40–60 min of every 100 min Hisaki orbit. This data acquisition continued through DOY21–243.

Following *Kimura et al.* [2015, 2016], the power emitted from the aurora is derived by 10 min integration of the imaging spectral data. The spectral region used for the integration spans from 900 to 1480 Å, and the spatial region of 20 arcsec from Jupiter's north pole is extracted. The contamination by disk emission was estimated to be ~150 GW when the northern aurora faces antiearthward [*Kimura et al.*, 2015].

The total emitted power of the torus is estimated in the same manner as the auroral analysis. The spectral range for the integration spans from 650 to 770 Å, where there is no significant geocoronal line emission [*Kuwabara et al.*, 2017]. This range corresponds to the line emissions of sulfur ions, S^+, S^{2+}, and S^{3+} (SIV 675 Å, SIII 680 Å, SIII 702 Å, SIII 729 Å, SIV 748 Å, and SII 765 Å). The photon production rate is positively correlated with the abundance of hot electrons at 10 s–100 s eV in the torus [e.g., *Delamere and Bagenal*, 2003; *Yoshioka et al.*, 2011, 2014; *Tsuchiya et al.*, 2015]. Two regions of interest are defined for the torus integration: the dawn and dusk ansae. The torus emission from the region at 20–200 arcsec (i.e., ~1–10 R_J around Jupiter's opposition) from the center of Jupiter is integrated over 10 min for the dawn and dusk, respectively.

The HST observing campaign spans from DOY137 to 200. During the campaign, HST took 44 images of the far ultraviolet (FUV) auroral emissions with the Space Telescope Imaging Spectrograph (STIS). The STIS imaging

was made with a 0.08 arcsec FWHM of PSF at 1300–1825 Å with the F25SRF2 filter. See *Nichols et al.* [2017] for further details.

3. Result

3.1. Transient Aurora on DOY142

Figure 1 shows a close-up of a transient aurora reaching to a peak power of 1.9 TW at 900 to 1480 Å on DOY 142 (see supporting information for observation in the entire analysis period on DOY136–160). This is one of the largest peak powers that have been measured throughout the entire Hisaki observing period from November 2013 to the present.

Figure 1a indicates the dependence of the auroral power during DOY140–144 on central meridian longitude (CML), shown with rainbow-colored error bars, and that of the average power during DOY1–240, shown with a black solid line. The average emission power excluding the transient event peaks around CML ~ 170°–230° [see also *Clarke et al.*, 1980; *Tao et al.*, 2016a, 2016b]. The transient auroral peak on DOY142, which was observed around CML ~ 260°, shown with a green error bar, is significantly above average by 10 standard deviations (10σ, where σ ~ 150 GW at CML ~ 260°). At this time, the northern magnetic pole of Jupiter faced the postnoon local time sector. Figure 1b shows the total auroral power (rainbow-colored error bars) with rotational modulation modeled with a sinusoidal function fitted to the observed power (red solid line). The period on DOY142.0–143.0 when the transient aurora occurred is excluded from the fit. The sinusoidal fit function represents the 9.925 h rotational modulation, which corresponds to the System III period, during the quiet period when no transient aurora was observed. Here we define the "onset" as the time at which the power exceeded 3σ above the average power versus CML (Figure 1a), which occurred on DOY142.1. HST took an image of the aurora just after the onset. After the onset, the auroral power reaches a peak of 1.9 TW, which is 10σ above the average CML dependence, on DOY142.2, and is followed by a "declining phase" where the power declined almost to the quiet emission power level within two rotations.

The auroral emission power from 1385 to 1448 Å where the emission is less absorbed by Jupiter's atmosphere is converted to the H_2 emission power that spans most of the UV wavelengths (700–1800 Å) eliminating Jupiter's atmospheric absorption and rotational modulation. The unabsorbed power estimation for the Hisaki data is established by *Tao et al.* [2016a, 2016b]. See these references for the details for the estimation. The unabsorbed emission power is ~8.5 TW, which corresponds to the total input power of ~85 TW. The unabsorbed emission power is approximately 4.5 times larger than that observed at 900–1480 Å, for the auroral peak on DOY142.

3.2. Dawn-Dusk Asymmetry in Torus

Based on the Hisaki monitoring of the dusk and dawn torus, *Tsuchiya et al.* [2015] detected periodicities at ~42.4 and ~9.9 h, which are close to Jupiter's rotation and Io's orbital period. They concluded that the detected periodicities are attributed to the hot electron populations associated with Io phase and Io's location with respect to the plasma torus. We model these periodicities with a linear sum of two offset sinusoidal functions at periods of 42.4 and 9.9 h. The modeled linear sums are shown with the red solid lines in Figures 1c and 1d. The offset, which is representative of the long-term averaged emission power, is estimated to be ~423 and 339 GW for the duskside and dawnside, respectively. It is notable that the rotational modulations in the dawn and dusk are in antiphase. The antiphase periodicity is also evident in the modulations around Io's orbital period.

It has been reported that the torus brightness sometimes indicates periodicities a few percent longer than Jupiter's rotation period [e.g., *Steffl et al.*, 2006]. To investigate the longer periodicities, the above fitting was also performed with a linear sum of two offset sinusoidal functions with a period of 42.4 h and that longer than 9.9 h (up to 10.3 h). There is no significant difference between fittings with the 9.9 h and longer periods. We conclude that periodicities in the torus brightness can be represented by periods of 42.4 and 9.9 h in this analysis period.

The torus emission power at the entire UV wavelength (0–1000 Å) is also estimated. The estimated power is approximated by multiplying the observed emission power by a factor ~ 2, which is the ratio of the entire wavelength power to the observed power evaluated based on the canonical EUV spectra as modeled by
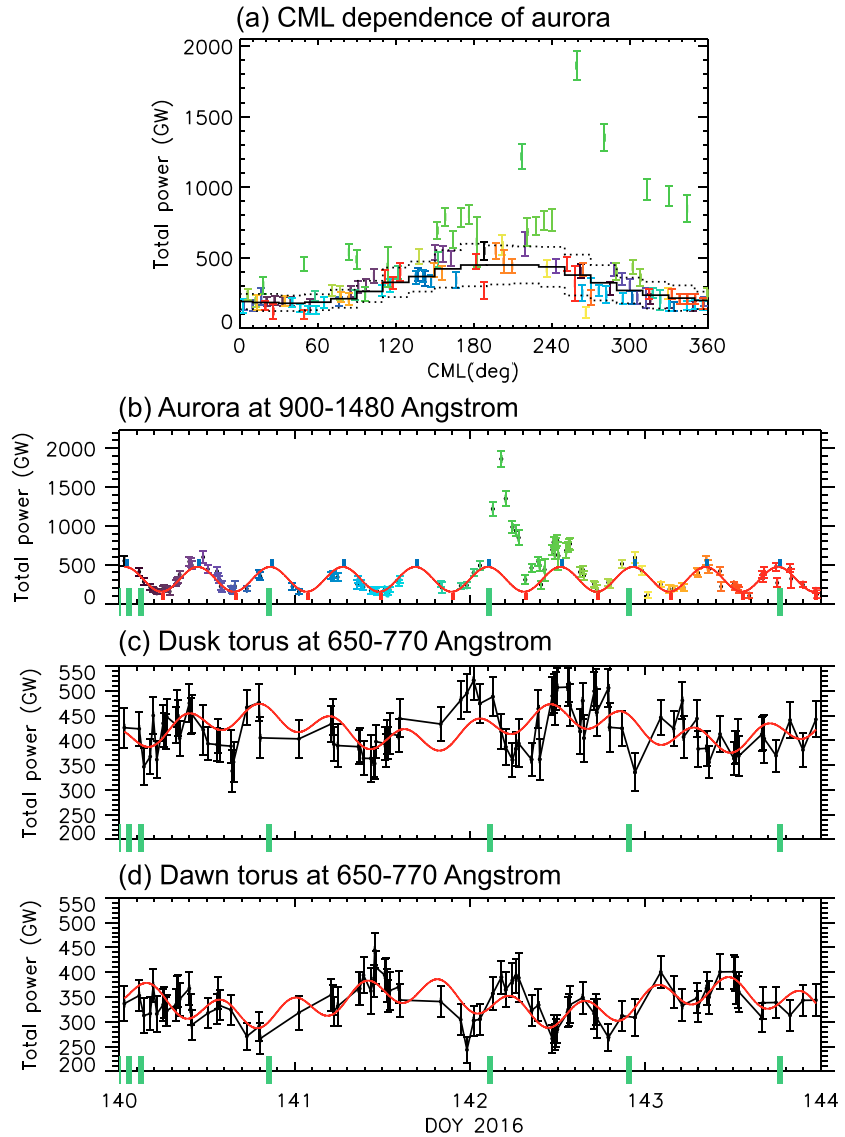
Figure 1. Close-up of the transient aurora on DOY142. (a) The emitted power of the aurora at 900–1480 Å as a function of the central meridian longitude (CML) of Hisaki. (b) The error in the power is estimated based on the photon statistics. The error bars are shown in the rainbow color scales corresponding to the observation time. The black solid line is the power averaged through 240 days from DOY1 to 240 in 2016 with total exposure time of 40.8 days. The dotted lines are the standard deviations on DOY1–240. The auroral power at 900–1480 Å as a function of time (Figure 1b). The red line is the rotational modulation modeled with a sinusoidal function $P_{aul} = P^{aul}_{rot} \sin\left(2\pi f_{rot} t + \phi^{aul}_{rot}\right) + P^{aul}_{dc}$ with frequency of a planetary rotation $f_{rot} = 1/9.925(1/h)$, time t, arbitrary initial phase ϕ^{aul}_{rot}, amplitude P^{aul}_{rot}, and offset P^{aul}_{dc}. P^{aul}_{rot} and P^{aul}_{dc} are estimated to be 153 and 315 GW, respectively. The blue ticks show the times when the northern aurora faces the observer (CML = 200°), while the red ticks show the opposite direction (CML = 20°). The green ticks show the HST imaging time. (c) The emitted power of the duskside torus at 650–770 Å. The modulations associated with Jupiter's rotation and Io's orbital period are modeled with a linear sum of two sinusoidal functions $P_{tor} = P^{tor}_{rot} \sin\left(2\pi f_{rot} t + \phi^{tor}_{rot}\right) + P^{tor}_{io} \sin\left(2\pi f_{io} t + \phi^{tor}_{io}\right) + P^{tor}_{dc}$ with similar parameters to the aurora. The amplitudes and offset are estimated by the fitting to be $P^{tor}_{rot} = 25$ and $P^{tor}_{io} = 23$ and $P^{tor}_{dc} = 423$ GW, respectively. (d) The emitted power for the dawnside torus at 650–770 Å in the same format as in Figure 1c with $P^{tor}_{rot} = 22$ and $P^{tor}_{io} = 26$ and $P^{tor}_{dc} = 339$ GW.

using the CHIANTI atomic database [e.g., *Steffl et al.*, 2004; *Yoshioka et al.*, 2011, 2014]. The emitted total power of the torus during the transient aurora is estimated to be ~1.5 TW.

The residual power of the aurora is obtained by subtracting the fitted sinusoidal function from the observed power (Figure 2a). The residuals for the torus are also obtained in the same manner (Figures 2c and 2d). The transient aurora spans from DOY142.1 to 142.8. This corresponds to the duration of ~17 h. Before the onset of
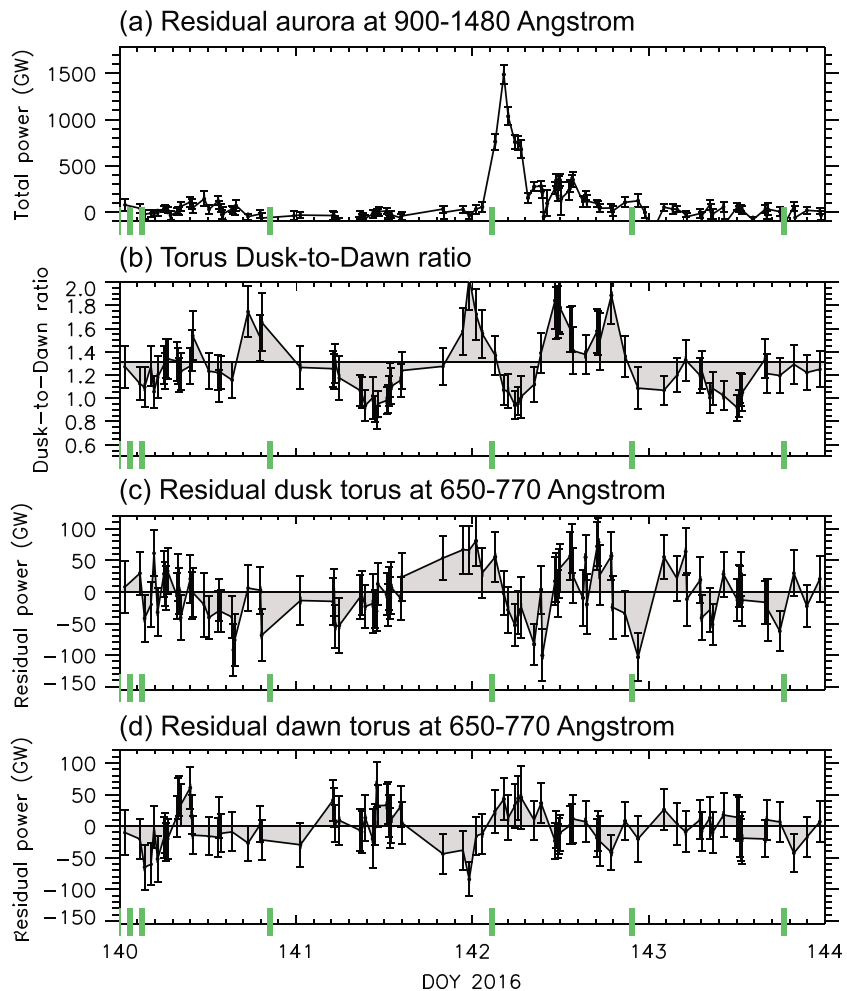
Figure 2. Residual powers of the aurora and torus. (a) The residual power of the aurora obtained by subtracting the fitted sinusoidal function from the observed power in Figure 1. (b) The ratio of the total duskside power to the dawnside. The horizontal solid line is the average of the ratio on DOY140.0–144.0. (c) The residual power of the duskside torus obtained by subtracting the fitted sinusoidal functions from the observed power in Figure 1. (d) The residual power of the dawnside torus in the same format as in Figure 2c.

the transient aurora, there are some modulations in the duskside and dawnside tori. The duskside residual (Figure 2c) positively deviates by <70 GW from the fitted function on DOY141.8–142.1 simultaneously with the negative deviation by <70 GW in the dawnside residual (Figure 2d). This variation more clearly appears in the ratio of the dusk total power to the dawn as the positive deviation from the average (Figure 2b). The positive deviation means that the dusk is brighter than its average. In contrast, the dawn is darker than the average. The dusk-to-dawn ratio shows local maxima on DOY142.0. This variation in the dusk-to-dawn ratio continues around the transient aurora: the maxima on DOY142.5 and 142.8 and minima on DOY142.25 and 142.65. From the temporal intervals between the local maxima and minima, the average periodicity is estimated to be ~9.6 h. It should be noted that the first pair of the maxima and minima on DOY142.0 and 142.25 is coincident with the antiphase residual power, while the second pair on DOY142.5 and 142.65 is only with the dusk residual enhancement; i.e., the dawn torus shows the average power.

3.3. Auroral Structure

Figure 3 shows the auroral images observed by HST on DOY140–142. The image taken on DOY140 is shown as a representative for the quiet period (Figure 3b). Between 02:17:42 and 03:02:12 (DOY142.10–142.13) on DOY142 (Figures 3c–3e), a dawn storm, which is suggestive of dawnside tail reconnection and planetward
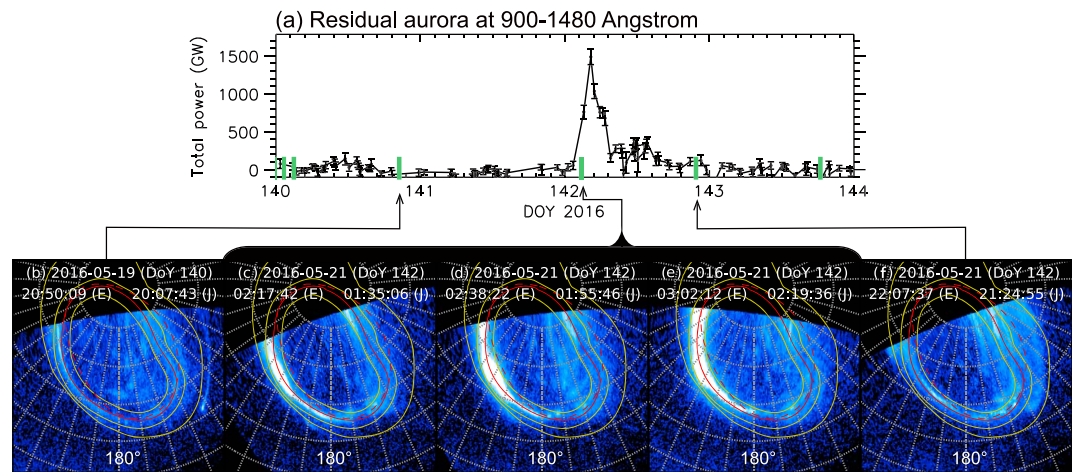
Figure 3. The polar projection of the FUV auroral image taken by HST/STIS on DOY140–142. The blue-to-white color scale spans from 1 to 3 MR in logarithmic scale. (a) The same panel as in Figure 2a. (b) The auroral image taken at 20:50:59 (HST observation time) on DOY140 (DOY140.87). The white grids show the longitude and latitude in System III coordinates with 10° intervals. The longitude of 180° is directed toward the bottom. The yellow solid lines are reference locations for the boundaries between the poleward region, main oval, and outer emissions. The statistical oval in this observation period is shown with a solid red line, while the latitude corresponding to the equatorial distance of 30 R_J in VIP4 magnetic field model [*Connerney et al.*, 1998] is shown with a red dashed line [see *Nichols et al.*, 2017]. The images taken at (c) 02:17:42, (d) 02:38:22, and (e) 03:02:12 (DOY142.10, 142.11, and 142.13). (f) The image taken at 22:07:37 (DOY142.92).

return flow [*Cowley et al.*, 2003; *Clarke et al.*, 2004], was evident at System III longitude of 180°–260° less than in the main oval (Figures 3c–3e) as observed during the 2014 HST campaign [*Kimura et al.*, 2015; *Badman et al.*, 2016; *Gray et al.*, 2016]. This exposure time corresponds to the onset timing of the transient aurora in the Hisaki data. The adjacent images in Figures 3c–3e indicate that the dawn storm rapidly expands in latitude and longitude and brightens from 2.2 to 5.5 TW within 44.2 min. It should be noted that this increase is attributed to both the temporal evolution of the total emission power and an increase in the apparent area of the corotating auroral structure. See *Nichols et al.* [2017] for details of the HST observations during this period.

The last HST image shown in Figure 3f was taken at 22:07:37 (DOY142.92) on DOY142 after the declining phase of the transient aurora when the auroral power in the Hisaki data had almost returned to the quiet level. The dawn storm in the main oval had dimmed. The outer emission appeared from System III longitude <100° to 150°. The dusk sector of the poleward emission at System III longitude of 150°–170° was also indicative of an enhancement.

4. Discussion

An enhancement in Jupiter's sodium nebula, which is associated with Io's volcanic eruption, was observed on DOY140 (M. Yoneda, private communication, 2017), as part of a long-term observing program from 2015 [*Yoneda et al.*, 2015]. We suggest that this may be associated with enhanced mass-loading and subsequent loss via tail reconnection. We therefore conclude that the transient aurora is partly internally driven associated with mass loading from Io, as reported by *Kimura et al.* [2015].

Based on the in situ solar wind measurements with Juno during the HST campaign, however, *Nichols et al.* [2017] reported that the solar wind forward shock arrived at Juno on DOY141.45. Juno was just upstream of Jupiter. It should be noted that the transient aurora in the present study could be associated with the shock arrival in parallel with the internal process. This solar wind response has been reported as auroral radio brightenings following shock arrivals [*Gurnett et al.*, 2002; *Hess et al.*, 2012, 2014]. Enhancements in decametric radio emission emitted from the duskside of northern polar region were frequently observed during forward shock arrivals [*Hess et al.*, 2012]. This could be associated with the enhancements in the outer and/or poleward emissions in the northern dusk sector observed in the present study (Figure 3f).

The long-term continuous monitoring of the aurora from 2013 to 2015 by *Kimura et al.* [2015, 2016] and *Kita et al.* [2016] indicated that the day-to-day variability in the aurora is well correlated with the solar wind shock arrival. These studies concluded that the transient aurora does not strongly depend on solar wind conditions. However, the present observation newly suggests that in this case the large transient aurora and energetic event would be excited by the combination of the internal and external processes; e.g., the mass and energy are stored via internal mass loading from Io, and the solar wind compression triggers the energy release via tail reconnection.

For the shock arrival on DOY141.45, we estimated the radial propagation time of the shock from Juno to the regions of interest: (a) the torus, (b) Jupiter, and (c) midnight tail region at 100 R_J from Jupiter. With a solar wind radial velocity of 475 km/s [*Nichols et al.*, 2017] and radial distance of 30 R_J between Juno and Jupiter in heliocentric coordinates, the propagation times (a)–(c) are estimated to be ~1, 1.3, and 5.4 h, respectively. These propagation times are significantly shorter than those between the shock arrival time at Juno and brightening of the transient aurora (DOY142.1), ~15.6 h. The initiation of the aurora brightening was delayed for ~10 h or more than the solar wind propagation time. Although the cause of the time lag of >10 h is still unknown, it might represent the amount of time it took to cause a large-scale reconnection of the tail and for the hot plasma to propagate around to the dawn.

The duskside and dawnside torus powers show both rotational periodicities and a transient brightening after the shock arrival on DOY141.45 (Figures 2b–2d). We observed the decrease in the dusk-to-dawn ratio on DOY141.5 and the dawn-dusk antiphase variability in the torus on DOY141.8–142.5, which lasted before the auroral onset through the declining phase. They were also likely affected by the dawn-dusk electric field modulation by the solar wind [*Murakami et al.*, 2016]. According to the above estimation of solar wind propagation, the dawn-dusk electric field was likely modulated by the solar wind variability associated with the forward shock on DOY141.45.

The transient brightening was observed in the dusk residual power on DOY142.50–142.65 (Figures 2b–2d). The dawn-dusk antiphase variability was less clear than that on DOY141.8–142.5. This suggests that a hot electron population appeared in the dusk torus at <10 R_J during the auroral declining phase and dissipated within ~1 rotation. With reference to previous works, this torus variability is likely associated with some combination of the following processes: energetic particle injection [e.g., *Mauk et al.*, 2002], adiabatic heating by the dawn-to-dusk electric field [*Barbosa and Kivelson*, 1983; *Murakami et al.*, 2016], and/or heating by electromagnetic waves originally proposed for Io's downstream region [*Hess et al.*, 2010; *Tsuchiya et al.*, 2015]. Although it is still unclear which process is the most feasible, the appearance of outer auroral emission at dusk after the declining phase of the transient aurora (Figure 3f) suggests that the energetic electron injection occurred after the transient aurora onset as reported from previous HST observations [*Gray et al.*, 2016]. Therefore, the transient dusk torus brightening on DOY142.50–142.65 is presumably associated with the injection.

The auroral images on DOY142.1 indicate the rapid evolution of the dawn storm in longitude and latitude at the onset of the transient aurora (Figures 3c–3e). Unfortunately, there is no imaging at the peak of the transient aurora in the present observation period. However, the auroral structure observed in the 2014 images at the time of peak power [*Kimura et al.*, 2015, Figure 3b; *Badman et al.*, 2016, Figure 1i; *Gray et al.*, 2016, Figures 1a–1e] indicates enhancements of both the dawn storm and intense blobby outer emissions. *Gray et al.* [2016] also reported that at the peak phase a significantly super-rotating polar spot was observed merging into the dawn storm from the nightside. During the declining phase, the imaging [*Kimura et al.*, 2015, Figure 3a; *Badman et al.*, 2016, Figure 1d] showed the disappearance of the dawn storm and the persistence of outer emission. The imaging of the postdeclining phase in the present study is indicative of the remnant outer emission at dusk (Figure 3f; see also Figure 1f in *Gray et al.* [2016]). In the current sequence of observations, *Nichols et al.* [2017] discovered pulsating duskside poleward emission, which they suggested is a manifestation of large-scale dusk/nightside reconnection as part of the Vasyliūnas or Dungey cycles.

Combining the present study with those of *Kimura et al.* [2015], *Badman et al.* [2016], *Gray et al.* [2016], and *Nichols et al.* [2017], the temporal evolution of the transient aurora is summarized as follows: onset phase: dawn storm initiation followed by expansion in latitude and longitude and rapid increase in the total power over a few hours; peak phase: continuing dawn storm, spot merging into the dawn storm, outer emission initiation, and total power peak; declining phase: dawn storm dissipation, continuing outer emission, and

total power declining within 1–2 rotations; and postdeclining phase: remnant outer emission, pulsating dusk-side poleward emission, and quiet level of the total power.

It should be noted that the initiation of the dawn storm is temporally followed by the outer emission. This strongly suggests that the sequence of the energetic event starts from the middle or outer magnetosphere and expands toward the inner magnetosphere within <1–2 rotations (sequences 1–3). *Gray et al.* [2016] interpreted the polar spot as the tail reconnection signature. The latitudinal shift as the spot merges into the dawn storm at the peak phase is suggestive of the radially inward transport of the hot plasma, which has been observed in *Galileo* in situ data frequently in the dawn tail [*Kronberg et al.*, 2008; *Kasahara et al.*, 2013]. The expanding dawn storm in the present study (Figures 3c–3e) is likely an evidence for region associated with the tail reconnection expanding in the radial and azimuthal directions at the onset phase. The transient dusk torus brightening during the declining phase (DOY142.5–142.65) is consistent with the several injection events in the central plasma torus during the transient aurora as reported by *Yoshikawa et al.* [2016]. Thus, we speculate that the energetic event is initiated by the tail reconnection and releases energy as the plasma inward flow at the onset phase of transient aurora, which is transported toward the inner magnetosphere up to the central plasma torus during the peak to declining phases.

With the radial distance of possible X-line of the dawn reconnection at ~60–100 R_J [*Woch et al.*, 2002; *Kasahara et al.*, 2013], the innermost radial distance of the injection at ~6 R_J, and the transport time scale of ~2.5 h (typical time difference between the onset and peak phase), the average velocity of the transport is estimated to be 430–750 km/s. This velocity range is comparable with the velocity of the ion jet front associated with the dawn tail reconnection, 380–550 km/s, directly measured with the particle instrument onboard Galileo [*Kasahara et al.*, 2013].

References

Badman, S. V., et al. (2016), Weakening of Jupiter's main auroral emission during January 2014, *Geophys. Res. Lett.*, *43*, 988–997, doi:10.1002/2015GL067366.

Barbosa, D. D., and M. G. Kivelson (1983), Dawn-dusk electric field asymmetry of the Io plasma torus, *Geophys. Res. Lett.*, *10*, 210–213, doi:10.1029/GL010i003p00210.

Bonfond, B., D. Grodent, J.-C. Gérard, T. Stallard, J. T. Clarke, M. Yoneda, A. Radioti, and J. Gustin (2012), Auroral evidence of Io's control over the magnetosphere of Jupiter, *Geophys. Res. Lett.*, *39*, L01105, doi:10.1029/2011GL050253.

Bonfond, B., D. Grodent, S. V. Badman, J.-C. Gérard, and A. Radioti (2016), Dynamics of the flares in the active polar region of Jupiter, *Geophys. Res. Lett.*, *43*, 11,963–11,970, doi:10.1002/2016GL071757.

Clarke, J. T., H. W. Moos, S. K. Atreya, and A. L. Lane (1980), Observations from Earth orbit and variability of the polar aurora on Jupiter, *Ap. J.*, *241*, L179–L182.

Clarke, J. T., D. Grodent, S. Cowley, E. Bunce, J. Connerney, and T. Satoh (2004), Jupiter's aurora, in *Jupiter. The Planet, Satellites and Magnetosphere*, edited by F. Bagenal, T. E. Dowling, and W. B. McKinnon, pp. 639–670, Cambridge. Univ. Press, Cambridge, U. K.

Connerney, J. E. P., M. H. Acuña, N. F. Ness, and T. Satoh (1998), New models of Jupiter's magnetic field constrained by the Io flux tube footprint, *J. Geophys. Res.*, *103*, 11,929–11,940.

Cowley, S. W. H., and E. J. Bunce (2003a), Modulation of Jovian middle magnetosphere currents and auroral precipitation by solar wind-induced compressions and expansions of the magnetosphere: Initial conditions and steady state, *Planet. Space Sci.*, *51*, 31–56, doi:10.1016/S0032-0633(02)00130-7.

Cowley, S. W. H., and E. J. Bunce (2003b), Modulation of Jupiter's main auroral oval emissions by solar wind induced expansions and compressions of the magnetosphere, *Planet. Space Sci.*, *51*, 57–79, doi:10.1016/S0032-0633(02)00118-6.

Cowley, S. W. H., E. J. Bunce, T. S. Stallard, and S. Miller (2003), Jupiter's polar ionospheric flows: Theoretical interpretation, *Geophys. Res. Lett.*, *30*(5), 1220, doi:10.1029/2002GL016030.

Delamere, P. A., and F. Bagenal (2003), Modeling variability of plasma conditions in the Io torus, *J. Geophys. Res.*, *108*(A7), 1276, doi:10.1029/2002JA009706.

Dumont, M., D. Grodent, A. Radioti, B. Bonfond, and J.-C. Gérard (2014), Jupiter's equatorward auroral features: Possible signatures of magnetospheric injections, *J. Geophys. Res. Space Physics*, *119*, 10,068–10,077, doi:10.1002/2014JA020527.

Gray, R. L., S. V. Badman, B. Bonfond, T. Kimura, H. Misawa, J. D. Nichols, M. F. Vogt, and L. C. Ray (2016), Auroral evidence of radial transport at Jupiter during January 2014, *J. Geophys. Res. Space Physics*, *121*, 9972–9984, doi:10.1002/2016JA023007.

Grodent, D. (2015), A brief review of ultraviolet auroral emissions on giant planets, *Space Sci. Rev.*, *187*, 23–50, doi:10.1007/s11214-014-0052-8.

Grodent, D., J.-C. Gérard, J. T. Clarke, G. R. Gladstone, and J. H. Waite Jr. (2004), A possible auroral signature of a magnetotail reconnection process on Jupiter, *J. Geophys. Res.*, *109*, A05201, doi:10.1029/2003JA010341.

Gurnett, D. A., et al. (2002), Control of Jupiter's radio emission and aurorae by the solar wind, *Nature*, *415*, 985–987.

Hess, S. L. G., P. Delamere, V. Dols, B. Bonfond, and D. Swift (2010), Power transmission and particle acceleration along the Io flux tube, *J. Geophys. Res.*, *115*, A06205, doi:10.1029/2009JA014928.

Hess, S. L. G., E. Echer, and P. Zarka (2012), Solar wind pressure effects on Jupiter decametric radio emissions independent of Io, *Planet. Space Sci.*, *70*, 114–125.

Hess, S. L. G., E. Echer, P. Zarka, L. Lamy, and P. Delamere (2014), Multi-instrument study of the Jovian radio emissions triggered by solar wind shocks and inferred magnetospheric subcorotation rates, *Planet. Space Sci.*, *99*, 136–148.

Hill, T. W. (1979), Inertial limit on corotation, *J. Geophys. Res.*, *84*, 6554.

Hill, T. W. (2001), The Jovian auroral oval, *J. Geophys. Res.*, *106*, 8101–8107, doi:10.1029/2000JA000302.

Kasahara, S., E. A. Kronberg, T. Kimura, C. Tao, S. V. Badman, A. Masters, A. Retinò, N. Krupp, and M. Fujimoto (2013), Asymmetric distribution of reconnection jet fronts in the Jovian nightside magnetosphere, *J. Geophys. Res. Space Physics*, *118*, 375–384, doi:10.1029/2012JA018130.

Khurana, K. K., M. G. Kivelson, V. M. Vasyliūnas, N. Krupp, J. Woch, A. Lagg, B. H. Mauk, and W. S. Kurth (2004), The configuration of Jupiter's magnetosphere, in *Jupiter, The Planet, Satellites and Magnetosphere*, edited by F. Bagenal, T. E. Dowling, and W. B. McKinnon, pp. 593–616, Cambridge. Univ. Press, Cambridge, U. K.

Kimura, T., et al. (2015), Transient internally driven aurora at Jupiter discovered by Hisaki and the Hubble Space Telescope, *Geophys. Res. Lett.*, *42*, 1662–1668, doi:10.1002/2015GL063272.

Kimura, T., et al. (2016), Jupiter's X-ray and EUV auroras monitored by Chandra, XMM-Newton, and Hisaki satellite, *J. Geophys. Res. Space Physics*, *121*, 2308–2320, doi:10.1002/2015JA021893.

Kita, H., et al. (2016), Characteristics of solar wind control on Jovian UV auroral activity deciphered by long-term Hisaki EXCEED observations: Evidence of preconditioning of the magnetosphere?, *Geophys. Res. Lett.*, *43*, 6790–6798, doi:10.1002/2016GL069481.

Kronberg, E. A., K.-H. Glassmeier, J. Woch, N. Krupp, A. Lagg, and M. K. Dougherty (2007), A possible intrinsic mechanism for the quasi-periodic dynamics of the Jovian magnetosphere, *J. Geophys. Res.*, *112*, A05203, doi:10.1029/2006JA011994.

Kronberg, E. A., J. Woch, N. Krupp, and A. Lagg (2008), Mass release process in the Jovian magnetosphere: Statistics on particle burst parameters, *J. Geophys. Res.*, *113*, A10202, doi:10.1029/2008JA013332.

Kuwabara, M., K. Yoshioka, G. Murakami, F. Tsuchiya, T. Kimura, A. Yamazaki, and I. Yoshikawa (2017), The geocoronal responses to the geomagnetic disturbances, *J. Geophys. Res. Space Physics*, *122*, 1269–1276, doi:10.1002/2016JA023247.

Louarn, P., C. P. Paranicas, and W. S. Kurth (2014), Global magnetodisk disturbances and energetic particle injections at Jupiter, *J. Geophys. Res. Space Physics*, *119*, 4495–4511, doi:10.1002/2014JA019846.

Mauk, B. H., J. T. Clarke, D. Grodent, J. H. Waite, C. P. Paranicas, and D. J. Williams (2002), Transient aurora on Jupiter from injections of magnetospheric electrons, *Nature*, *415*, 1003–1005, doi:10.1038/4151003a.

Murakami, G. K. Y., et al. (2016), Response of Jupiter's inner magnetosphere to the solar wind derived from extreme ultraviolet monitoring of the Io plasma torus, *Geophys. Res. Lett.*, *43*, 12,308–12,316, doi:10.1002/2016GL071675.

Nichols, J. D., et al. (2017), Response of Jupiter's auroras to conditions in the interplanetary medium as measured by the Hubble Space Telescope and Juno, *Geophys. Res. Lett.*, *44*, doi:10.1002/2017GL073029, in press.

Pallier, L., and R. Prangé (2001), More about the structure of the high latitude Jovian aurorae, *Planet. Space Sci.*, *49*, 1159–1173.

Pallier, L., and R. Prangé (2004), Detection of the southern counterpart of the Jovian northern polar cusp: Shared properties, *Geophys. Res. Lett.*, *31*, L06701, doi:10.1029/.2003GL018041.

Prangé, R., G. Chagnon, M. G. Kivelson, T. A. Livengood, and W. Kurth (2001), Temporal monitoring of Jupiter's auroral activity with IUE during the Galileo mission. Implications for magnetospheric processes, *Planet. Space Sci.*, *49*, 405–415, doi:10.1016/S0032-0633(00)00161-6.

Pryor, W. R., et al. (2005), Cassini UVIS observations of Jupiter's auroral variability, *Icarus*, *178*, 312–326, doi:10.1016/j.icarus.2005.05.021.

Radioti, A., A. T. Tomás, D. Grodent, J.-C. Gérard, J. Gustin, B. Bonfond, N. Krupp, J. Woch, and J. D. Menietti (2009), Equatorward diffuse auroral emissions at Jupiter: Simultaneous HST and Galileo observations, *Geophys. Res. Lett.*, *36*, L07101, doi:10.1029/2009GL037857.

Steffl, A. J., A. Ian, F. Stewart, and F. Bagenal (2004), Cassini UVIS observations of the Io plasma torus: I. Initial results, *Icarus*, *172*(1), 78–90, doi:10.1016/j.icarus.2003.12.027.

Steffl, A. J., P. A. Delamere, and F. Bagenal (2006), Cassini UVIS observations of the Io plasma torus III. Observations of temporal and azimuthal variability, *Icarus*, *180*, 124–140.

Tao, C., T. Kimura, S. V. Badman, N. André, F. Tsuchiya, G. Murakami, K. Yoshioka, I. Yoshikawa, A. Yamazaki, and M. Fujimoto (2016a), Variation of Jupiter's aurora observed by Hisaki/EXCEED: 1. Observed characteristics of the auroral electron energies compared with observations performed using HST/STIS, *J. Geophys. Res. Space Physics*, *121*, 4041–4054, doi:10.1002/2015JA021271.

Tao, C., T. Kimura, S. V. Badman, N. André, F. Tsuchiya, G. Murakami, K. Yoshioka, I. Yoshikawa, A. Yamazaki, and M. Fujimoto (2016b), Variation of Jupiter's aurora observed by Hisaki/EXCEED: 2. Estimations of auroral parameters and magnetospheric dynamics, *J. Geophys. Res. Space Physics*, *120*, 4055–4071, doi:10.1002/2015JA021272.

Tomás, A. T., J. Woch, N. Krupp, A. Lagg, K.-H. Glassmeier, and W. S. Kurth (2004), Energetic electrons in the inner part of the Jovian magnetosphere and their relation to auroral emissions, *J. Geophys. Res.*, *109*, A06203, doi:10.1029/2004JA010405.

Tsuchiya, F., et al. (2010), Plan for observing magnetospheres of outer planets by using the EUV spectrograph onboard the SPRINT-A/EXCEED mission, *Adv. Geosci.*, *25*, 57–71, doi:10.1142/9789814355377_0005.

Tsuchiya, F., et al. (2015), Local electron heating in the Io plasma torus associated with Io from HISAKI satellite observation, *J. Geophys. Res. Space Physics*, *120*, 10,317–10,333, doi:10.1002/2015JA021420.

Vasyliūnas, V. M. (1983), Plasma distribution and flow, in *Physics of the Jovian Magnetosphere*, edited by A. J. Dessler, pp. 395–453, Cambridge Univ. Press, New York.

Waite, J. H., Jr., et al. (2001), An auroral are at Jupiter, *Nature*, *410*, 787–789, doi:10.1038/35071018.

Woch, J., N. Krupp, and A. Lagg (2002), Particle bursts in the Jovian magnetosphere: Evidence for a near-Jupiter neutral line, *Geophys. Res. Lett.*, *29*(7), 1138, doi:10.1029/2001GL014080.

Yamazaki, A., et al. (2014), Field-of-view guiding camera on the HISAKI (SPRINT-A) satellite, *Space Sci. Rev*, *184*, 259–274, doi:10.1007/s11214-014-0106-y.

Yoneda, M., M. Kagitani, F. Tsuchiya, T. Sakanoi, and S. Okano (2015), Brightening event seen in observations of Jupiter's extended sodium nebula, *Icarus*, *261*, 31–33, doi:10.1016/j.icarus.2015.07.037.

Yoshikawa, I., et al. (2016), Properties of hot electrons in the Jovian inner magnetosphere deduced from extended observations of the Io plasma torus, *Geophys. Res. Lett.*, *43*, 11,552–11,557, doi:10.1002/2016GL070706.

Yoshioka, K., G. Murakami, F. Tsuchiya, M. Kagitani, and I. Yoshikawa (2011), Hot electron component in the Io plasma torus confirmed through EUV spectral analysis, *J. Geophys. Res.*, *116*, A09204, doi:10.1029/2011JA016583.

Yoshioka, K., G. Murakami, A. Yamazaki, F. Tsuchiya, M. Kagitani, T. Sakanoi, T. Kimura, K. Uemizu, and I. Yoshikawa (2013), The extreme ultraviolet spectroscope for planetary science, EXCEED, *Planet. Space Sci.*, *85*, 250–260, doi:10.1016/j.pss.2013.06.021.

Yoshioka, K., et al. (2014), The evidence for the global electron transportation into the Jovian inner magnetosphere, *Science*, *345*(6204), 1581–1584, doi:10.1126/science.1256259.